Available online at www.sciencedirect.com
ScienceDirect
Acta Materialia 54 (2006) 4415–4426
Acta MATERIALIA
www.actamat-journals.com

Threshold stress superplastic behavior and dislocation activity in a three-phase alumina–zirconia–mullite composite

Tiandan Chen, Farghalli A. Mohamed, Martha L. Mecartney *

Department of Chemical Engineering and Materials Science, University of California, Irvine, CA 92697-2575, USA

Received 27 April 2006; accepted 1 May 2006
Available online 22 August 2006

Abstract

Creep tests were performed in compression on a three-phase alumina–zirconia–mullite composite in the temperature range 1673–1773 K. The data show steady-state deformation behavior with a high-strain rate. Plots of strain rate versus applied stress on a logarithmic scale exhibit a sigmoidal relationship, i.e., an increase of stress exponent with a decrease in applied stress. It is shown that such an increase in the stress exponent with increasing stress can be correlated with the existence of a threshold stress, which decreases with increasing temperature. Transmission electron microscopy studies reveal dislocation activity in some grains of the deformed material, which was not present in the as-sintered materials, indicating that dislocations were generated during deformation. These results, which are similar in trend to those reported for superplastic metallic alloys, lead to the conclusion that dislocation motion plays a role in accommodating grain boundary sliding in this material.

Keywords: Transmission electron microscopy; Ceramics; Dislocations; Superplasticity; High-temperature deformation

1. Introduction

Since superplastic flow in ceramic materials was reported by Wakai et al. [1,2], significant advances in the development of superplastic ceramics have been made, including extensive deformations of over 1000% for a 5 wt.% SiO_2-doped tetragonal zirconia (3Y-TZP) at 1673 K [3] and over 500% for 5 wt.% SiO_2-doped cubic zirconia (8Y-CSZ) at 1703 K [4]. More recently, a three-phase zirconia–alumina–spinel achieved more than 1000% deformation with a high-strain rate of 0.4 s^{-1} at 1923 K [5]. However, despite many advances in superplastic ceramic materials development, there is no consistent agreement on the deformation mechanism for superplasticity in ceramics.

Superplasticity in ceramics was widely reported years after the discovery of superplasticity in metals [1,6]. The more recent study of deformation behavior in ceramics has benefited from the prior achievements in micrograin superplasticity in metals. However, several common characteristics of superplasticity in metals including the occurrence of dislocation motion as an accommodation mechanism for sliding and the presence of a sigmoidal relationship between strain rate and stress are neither often reported nor accepted in ceramics, especially for alumina-based ceramics.

By contrast, grain boundary sliding accommodated by dislocation motion is accepted as a primary deformation mechanism in metals, although the details and assumptions of the accommodation process in various models are different [7–9]. Dislocation motion has often been ruled out as an accommodation mechanism in ceramics for two main reasons [10,11]. First, most transmission electron microscopy (TEM) studies have reported that the deformed microstructure in superplastic ceramics, including 3Y-TZP [12], 8Y-CSZ [13], and alumina [14] was dislocation free or contained very limited isolated dislocations, and

* Corresponding author.
E-mail address: martham@uci.edu (M.L. Mecartney).

1359-6454/$30.00
doi:10.1016/j.actamat.2006.05.002

many TEM investigations did not mention whether there were dislocations present in the deformed materials. Second, the stress to generate dislocations based on theoretical calculations [10] and single-crystal creep experiments [11] was much higher than the applied stress in most cases.

However, the absence of evidence regarding dislocations in ceramics after deformation is not evidence of the absence of dislocation activity during high-temperature deformation. Xun and Mohamed [15] have shown that for metal superplasticity, dislocations can rapidly migrate into the grain boundaries, and only the presence of pinning particles effectively traps dislocations so they can be seen during subsequent TEM studies. In addition, it is not clear whether the experimental procedures employed in previous studies in ceramics are valid for retaining dislocations. Dislocation features and the dislocation density revealed under TEM can be influenced by the deformation technique and TEM sample preparation methods. To preserve the deformed microstructure and dislocation activity, the deformed material needs to be cooled under load [16]. This step was not often taken.

Recently, dislocation activity in deformed ceramics has been reported in several studies. A high-strain rate and extensive strain in a three-phase zirconia–alumina–spinel were attributed to both limited grain growth and plastic deformation within zirconia grains [5]. TEM micrographs of this material showed developed dislocation structures in the zirconia phase. Additional observations of dislocations have been reported in deformed 3Y-TZP by Morita et al. [16,17] and Duclos and Crampon [18]. Morita et al. [19] also reported dislocation activity in deformed polycrystal $MgAl_2O_4$ and proposed that the dislocation motion could relax the stress concentration generated from boundary sliding. Strain hardening and a subsequent softening phenomenon were ascribed to an increase and decrease of the dislocation density. Dislocations were observed in both TZP and spinel in a deformed ZrO_2–30 vol.% $MgAl_2O_4$ superplastic composite, and the yield drop was attributed to a sharp increase in mobile dislocation in the spinel [20]. Dislocation sub-boundaries, formed from a shot blasting technique at room temperature, can significantly improve the fracture toughness of ceramics [21]. All these studies suggest that the role of dislocations should not be ignored in ceramics.

A sigmoidal relationship between strain rate and stress is another common characteristic in superplastic metals [22]. The increase of stress exponent in the low stress region is thought to be due to the existence of threshold stress. The concept of a threshold stress in superplastic metals was first introduced by Johnson [23] followed by experimental verification by Burton [24] in a superplastic Pb–Sn system. These authors were the first to suggest that the difference between regions I and II was not due to different deformation processes, but caused by the presence of a threshold stress whose significance increases with decreasing applied stress. Ashby and Verrall [25] and Gittus [26] further developed theories of superplasticity incorporating the concept of a threshold stress, speculating that the interaction between boundary dislocations and obstacles in the grain boundary (ledges and precipitates) could serve as the origin of the threshold stress. The threshold stresses predicted by these models exhibit a very weak temperature dependence; the temperature dependence of the threshold stress was expected to be the same as that of the shear modulus. As a result, these earlier models failed to explain the strong dependence of the threshold stress on temperature in superplastic metals as documented by experiments. Mohamed [27,28] was the first to attribute the threshold stress to the segregation of impurities at boundaries, a model that fits the exponential temperature dependence observed in experiments in superplastic metal alloys.

However, low stress creep data in ceramics are not often reported, especially for alumina-based materials; thus the sigmoidal relation was rarely reported in the past for ceramics. One exception is for yttria-stabilized tetragonal zirconia (TZP), where the presence of a threshold stress has been documented [29]. The threshold stress was observed to be dependent on the purity of the TZP material. More recent publications suggest that segregation (excess yttrium ions) at the grain boundaries is the cause of the threshold stress in TZP, similar to metallic systems [30,31]. The concept of a threshold stress in ceramics, however, has not been universally accepted. Calculations by other researchers using experimental data for TZP have yielded a negative threshold stress [32,33]. A negative value for the threshold stress causes the exclusion of the threshold stress approach in ceramics.

It is clear from the preceding summary that guiding information on dislocation activity and creep characteristics at low stresses in ceramics under superplastic conditions is needed to shed light on the origin and details of the mechanism of superplasticity in these materials. In an attempt to obtain such information, a detailed investigation was undertaken in which the creep and substructure of a three-phase alumina (40 vol.%)–zirconia (30 vol.%)–mullite (30 vol.%) ceramic composite at low stresses are examined for the first time. It is the purpose of the present paper to report and discuss the results of this investigation with a focus on the role of dislocations in accommodating grain boundary sliding.

2. Experimental

2.1. Material

The material used in this investigation is a three-phase alumina (40 vol.%)–zirconia (30 vol.%)–mullite (30 vol.%). For the sake of brevity, this material will be referred to as AZ30M30. AZ30M30 was selected for several reasons. First, it has been shown that the three-phase AZ30M30 exhibits steady-state deformation under constant compressive stress, which indicates the absence of significant grain growth during high-temperature deformation [34]. In particular, scanning electron microscopy (SEM) observations

show the presence of only very limited grain growth even after a true strain of 100% at 1723 K. Second, AZ30M30 exhibits a high-strain rate of $1.3 \times 10^{-2}\,s^{-1}$ at 1773 K and 60 MPa [34]. In general, a strain rate of $10^{-2}\,s^{-1}$ or greater is regarded as characteristic of a high-strain rate material. Third, both SEM and density measurements show no signs of cavitation after a strain of 100%. The steady-state strain rate, high-strain rate, and lack of cavitation indicate that AZ30M30 is a very promising superplastic ceramic composite.

2.2. Mechanical testing

AZ30M30 was prepared from nanoscale powders of high-purity alumina and zirconia (3Y-TZP) and a silica sol. The mullite phase formed from the reaction between alumina and silica. The sintered specimen was deformed under different compressive stresses and temperatures using a commercially available Applied Test System (ATS). The strain rate was calculated from the displacement versus time. Details about the sample preparation and deformation tests are presented in Refs. [34,35].

2.3. Microstructure examination

The microstructure of the as-sintered and deformed specimens was carefully inspected. Selected deformed specimens were deformed to 50% strain at 1723 K and 30 MPa and then cooled under loading conditions. Cooling water and a fan were employed to accelerate the cooling after deformation.

TEM specimens were prepared using a standard technique, involving mechanical grinding to a thickness of 100 μm, further dimpling down to a thickness about 15 μm and then ion bean milling to electron transparency at 6.5 kV. The deformed TEM thin disk was cut from the plane normal to the compression stress. TEM observations were performed using on a Philips CM20 (200 kV) instrument.

3. Results

3.1. Deformation characteristics

3.1.1. Stress dependence of steady-state creep rate

Fig. 1(a) in which creep rate is plotted against applied stress on a double logarithmic scale describes the stress dependence of steady-state creep rate in AZ30M30 for three different temperatures: 1673, 1723, and 1773 K. All strain rate data points plotted in Fig. 1(a) were collected after steady-state creep was reached. The stress exponent can be calculated from the slope of the plot and is equal to the reciprocal of the strain rate sensitivity. The change of stress exponent with decreasing applied stress is apparent from the plot that can be divided into two regions: region I and region II. At stresses higher than about 20 MPa (region II), the stress exponent has an n-value that

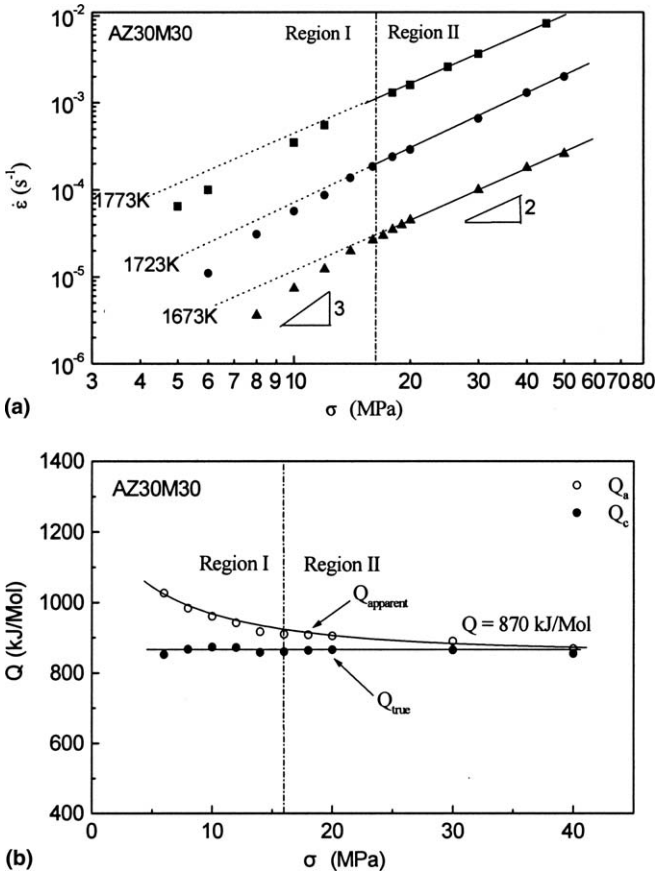

Fig. 1. (a) Steady-state strain rate is plotted as a function of applied stress at 1673, 1723, and 1773 K. (b) Apparent (Q_a) and true (Q_c) activation energy for creep are plotted as a function of applied stress (σ).

is independent of testing temperature and that is equal to about 2. An n-value of 2 agrees well with the values obtained in previous studies of alumina materials [36,37]. At stresses lower than about 20 MPa (region I), the stress exponent exhibits a value higher than 2. If the data at low stresses are fitted with straight lines, the following values of the stress exponent are obtained: 3.0, 2.9, and 2.5 at 1673, 1723, and 1773 K, respectively. Due to the limitation of the testing facility, the strain rates at high stresses were not accessible, so it was not feasible to determine whether there was a change of stress exponent for creep in AZ30M30 at applied stresses higher than 50 MPa.

3.1.2. Temperature dependence of the creep rate

The steady-state creep rate versus stress data in Fig. 1(a) were used to plot the logarithmic strain rate against $1/T$, where T is absolute temperature, at constant stress. The apparent activation energy for creep, Q_a, was then inferred from the slopes of resultant straight lines that are equal to Q_a/R, where R is the gas constant. The estimated values of Q_a are plotted as a function of the applied shear stress in Fig. 1(b). Inspection of the figure shows the following two features. First, the apparent activation energy, Q_a, is in general not constant but increases with decreasing applied stress. Second, the data can be divided into two

regions that parallel those related to the variation in the stress exponent with applied stress (Fig. 1(a)): (a) region II in which Q_a, decreases slowly with increasing stress approaching a constant value of about 870 kJ/mol, and (b) region I in which Q_a decreases rapidly with decreasing stress.

3.2. Microstructure

A careful inspection of the representative microstructure of the as-sintered and deformed materials revealed the following features.

3.2.1. Initial microstructure

Fig. 2 shows bright-field TEM micrographs of AZ30M30 in the as-sintered state with an average grain size of about 0.4 μm. The grains are nearly equiaxed, and most of the grain boundaries are sharply facetted (Fig. 2(a)). Although the amount of doped silica was 5.9 wt.% in the starting material prior to the formation of mullite, only a few very small glass pockets (10–15 nm size) at grain junctions were found (Fig. 2(b)). The initial microstructure is nearly dislocation free. Only a very few isolated dislocations were observed within the limited zirconia grains. The dislocations found in the as-sintered materials could be due to the extensive ball milling or thermal expansion mismatch. High strain is evident in some TZP grains due to TZP transformation from the tetragonal to monoclinic phase.

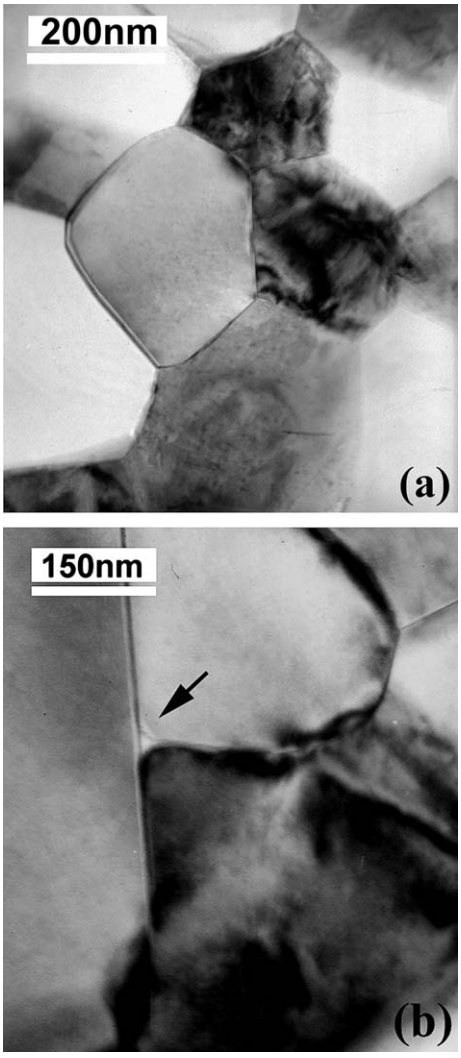

Fig. 2. TEM micrographs for the as-sintered materials: (a) typical grain shapes and (b) one of the few residual silica glassy pockets (10–15 nm).

3.2.2. Deformed microstructure

TEM observations of 50% deformed specimens show that grains remained primarily equiaxed. No sign of cavitation was observed in deformed AZ30M30 samples. The lack of observable cavitation was also confirmed by density measurements. However, for deformed specimens, strain contrast and bend contours appear pronounced, suggesting a high amount of strain energy in the specimen. Although most previous TEM studies have reported no dislocation activity in superplastic ceramics [12–14], a much higher density of dislocations was found in AZ30M30 after deformation. Dislocation activity and features in the mullite, zirconia, and alumina grains are described in the following sections. Energy dispersive spectroscopy (EDS) was used to verify the phase composition of individual grains.

3.2.2.1. Dislocations in mullite. Most dislocations were found in mullite grains. Representative dislocations in mullite are shown in Fig. 3. Dislocations were visible in some grains, while other grains appear free of dislocations. Dislocations were mainly present inside the mullite grains, and only a few were found along mullite boundaries.

Frequently, dislocations in mullite appeared to initiate from grain boundaries (triangles in Figs. 3(a) and (c)). Dislocations in mullite often traversed the grain, starting from one boundary and ending at the opposite boundary. Although a high density of dislocations was present in mullite grains, no entanglement of dislocations in mullite was found during these TEM investigations.

If there is a dispersion of small particles, precipitates, or impurity atoms in the microstructure, the moving dislocations will be pinned, and thus form a curved shape [15]. In Fig. 3(d), a curved dislocation pileup was revealed. These curved dislocations in mullite in the deformed AZ30M30 ceramic provide evidence for dislocation motion during deformation.

3.2.2.2. Dislocations in zirconia. Fig. 4 includes TEM micrographs that show dislocations in zirconia grains. Unlike dislocations in mullite grains, dislocations in zirconia do not often pile up within the grains [17]. Fig. 4(a) shows typical images for zirconia after deformation. In addition to the strain contrast of intragranular dislocations and twin boundaries (from the tetragonal to monoclinic transformation), there is strain contrast from grain boundary dislocations, also reported by Morita and Hiraga [38]. Fig. 4(b) shows a dislocation pile-up along one zirconia

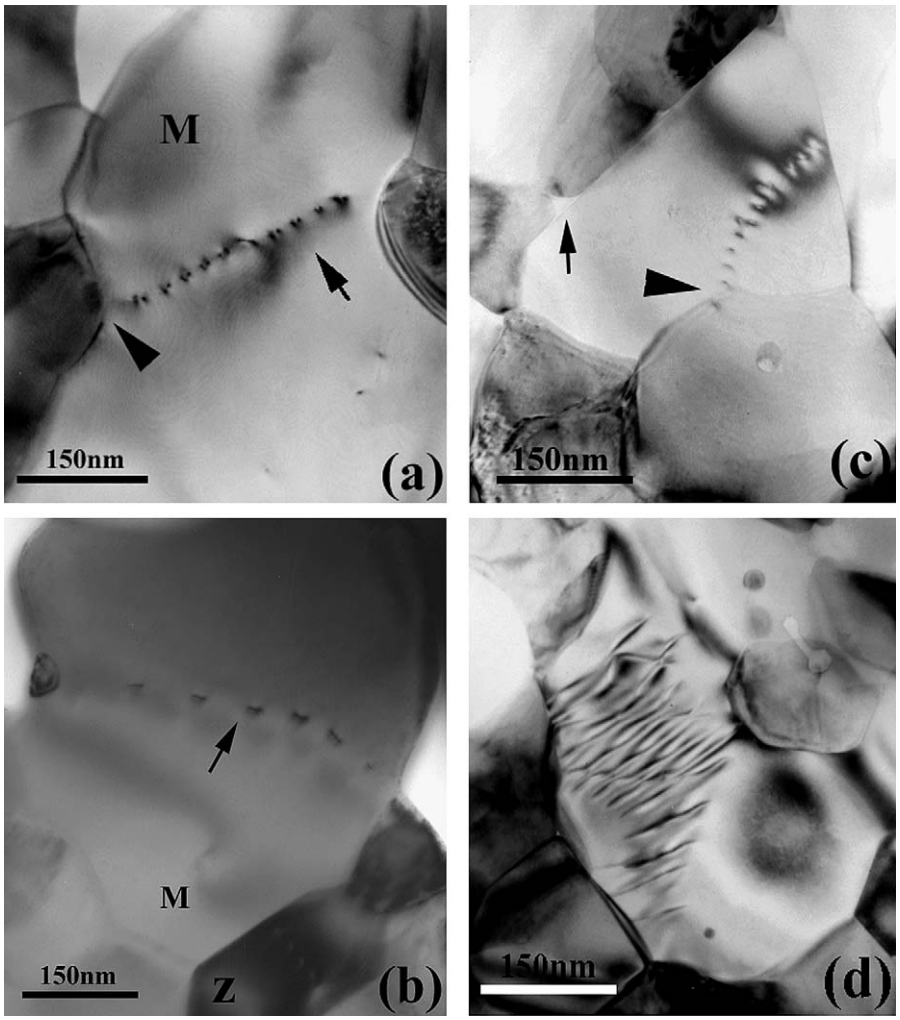

Fig. 3. TEM micrographs of dislocations in mullite grains: (a) dislocations pile-up between boundaries; (b) dislocations associated with small precipitate and junctions; (c) dislocation starts from the protrusion of nearby grain (triangle) and a tiny glass pocket is visible (arrow); (d) curved dislocations shape as the direct evidence of dislocation motion during high-temperature deformation.

grain boundary, together with two dislocation pile-ups in the nearby two mullite grains. Dislocations in zirconia were also recently reported by Kim et al. [5] in a three-phase zirconia–alumina–spinel ceramic and by Morita et al. [16,17] in tetragonal zirconia and zirconia–spinel composites [20].

3.2.2.3. Dislocations in alumina. The overall density of dislocations in alumina grains is lower than those in mullite and zirconia grains, which may be due to the fact that the elastic modulus of alumina is almost a factor of 2 higher than that of zirconia or mullite and there are fewer easy slip systems for Al_2O_3. (Easy slip is primarily on the basal plane at high temperature.) Fig. 5 provides dark-field images that show dislocations in an alumina grain. The dislocations shown in Fig. 5(a) are wavy in shape, serving as evidence for dislocation motion during deformation. Fig. 5(b) shows a dislocation pile-up associated with grain junctions. The wide white lines may be stacking faults between two partial dislocations or a result of $g \cdot b = 2$ imaging conditions.

It is worth emphasizing that all specimens were prepared for TEM examination using the same technique and under the same conditions. Accordingly, the apparent difference in the density of dislocations between the as-sintered and deformed specimens indicates that dislocations observed in the deformed materials are not artifacts, but generated during high-temperature deformation. The absence of dislocations in many previous published studies may due to three reasons: (a) the TEM samples were prepared from fractured specimens; (b) the deformed specimens were cooled down slowly under no loading conditions; and (c) researchers did not look for dislocations in deformed specimens due to the assumption that there would be no dislocations in the deformed materials. In cases (a) and (b), during the cooling, the dislocations could be recovered after the applied stress was removed and thus dislocations could disappear. Dislocations only need to travel a very short distance of less than 1 μm to be lost at nearby grain boundaries during unloading, cooling to room temperature, and subsequent specimen preparation for TEM examination.

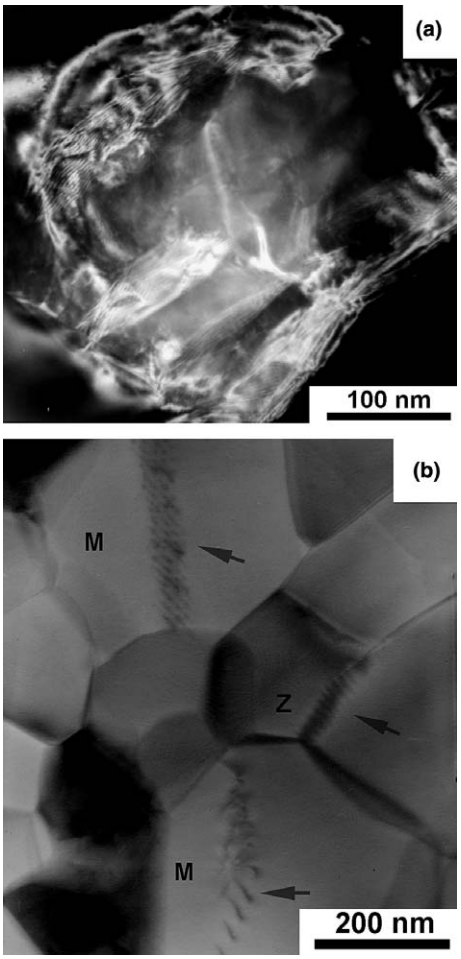

Fig. 4. TEM micrographs of dislocations in zirconia grains: (a) typical dislocations in zirconia grains along with twinning from the tetragonal to monoclinic phase transformation and (b) two dislocation pile-ups in mullite grains and one dislocation pile-up along a zirconia grain boundary.

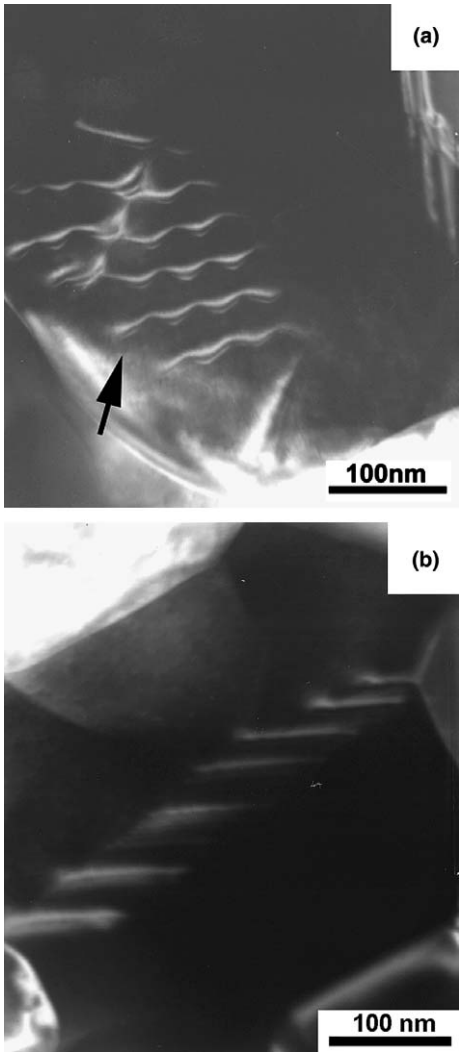

Fig. 5. Dark-field TEM micrographs of dislocations in alumina grains: (a) curved dislocation shape, indicating dislocations were moving during deformation and (b) dislocation pile-up.

4. Discussion

4.1. Threshold stress approach

An important characteristic of the creep behavior of micrograin superplastic metallic alloys is the experimental observation that the relationship between applied stress and steady-state strain rate at constant temperature is often sigmoidal [22,28]. This sigmoidal relationship is manifested by the presence of three regions: region I (the low-stress region), region II (the intermediate-stress region), and region III (the high-stress region). The characterization of the sigmoidal trend in terms of these regions is mainly based on the value of the stress exponent, $n(n = \partial \ln \dot{\varepsilon}/\partial \ln \sigma)$ at constant temperature and grain size. As reported elsewhere [22,28], the values of the stress exponent, n, and the activation energy for superplastic flow in regions I and III are higher than those in region II ($n \approx 2$, $Q \approx Q_{gb}$, where Q_{gb} is the activation energy for boundary diffusion) that is associated with maximum ductility (the superplastic region).

As mentioned earlier, due to the limitation of the testing facility, strain rates at high stresses were not accessible, so it is not known whether there is a change of stress exponent for creep in AZ30M30 at stresses higher than about 50 MPa. Despite this limitation, the emergence of a low-stress region (region I) with a higher value of stress exponent and a higher value of the apparent activation energy is apparent from Figs. 1(a) and (b). The relationship between region II ($n \approx 2$) and region I ($n > 2$) resembles in trend that characterizing superplastic flow in metallic systems [22,28] in the intermediate-stress region and the low-stress region, respectively, as summarized above. In addition, there are three other similarities in creep behavior between AZ30M30 and superplastic metallic systems such as Zn–22% Al. First, the stress exponent for creep in AZ30M30, like that reported for Zn–22% Al [22,28], in region II is about 2. Second, an examination of Fig. 1(a) shows that the deviation from region II to region I, like that associated with Zn–22% Al [28], shifts to higher strain

rates with increasing test temperature. Third, the variation in the apparent activation energy with applied stress for AZ30M30 as depicted in Fig. 1(b) stress mirrors in trend those reported for the superplastic Zn–22% Al [28] and Pb–62% Sn [39] alloys.

An increasing n-value with decreasing applied stress in superplastic metallic alloys such as Zn–22% Al [28] and Pb–62% Sn [39] has been explained in terms of the existence of a threshold stress, σ_0. However, the results related to the presence a threshold stress for superplastic flow in ceramics are in conflict. On the one hand, the possibility of a threshold stress was ruled out in previous studies on ceramics because the results yielded a negative σ_0 value [32,33]. On the other hand, Jimenez-Melendo et al. [40] and Morita et al. [41] studied the deformation behavior of TZP and reported positive values for σ_0. In order to examine whether the concept of a threshold stress is applicable to the description of the creep behavior of AZ30M30, a procedure similar to that applied elsewhere [28,39] was adopted. In this case, the data at a single temperature were plotted as $\dot{\varepsilon}^{-1/n}$ against σ on a double linear scale. Under the condition that a threshold exists and that its value is constant for each test temperature (independent of applied stress), the datum points of the aforementioned plot should fit a straight line whose extrapolation to zero strain rate yields the value of σ_0 at each temperature. Fig. 6 shows the plot of $\dot{\varepsilon}^{1/n}$ versus σ at three temperatures 1673, 1723, and 1773 K for $n = 2$. Consideration of this figure shows three findings. First, intercepts of the straight lines fitting the data with the stress axis yield the following positive values for the threshold stress: 2.5, 1.8, and 0.8 MPa at 1623, 1673, and 1723 K, respectively. Second, the threshold stress is sensitive to temperature as its value decreases with increasing temperature. This finding, which is similar to those reported for the superplastic Zn–22% Al [28] and Pb–62% Sn [39], establishes that the similarity in creep behavior between AZ30M30 and Zn–22% Al [28] is not confined to the observation of a sigmoidal relationship between stress and strain rate (regions I and II) but it extends to including the presence and characteristics of a threshold stress for deformation.

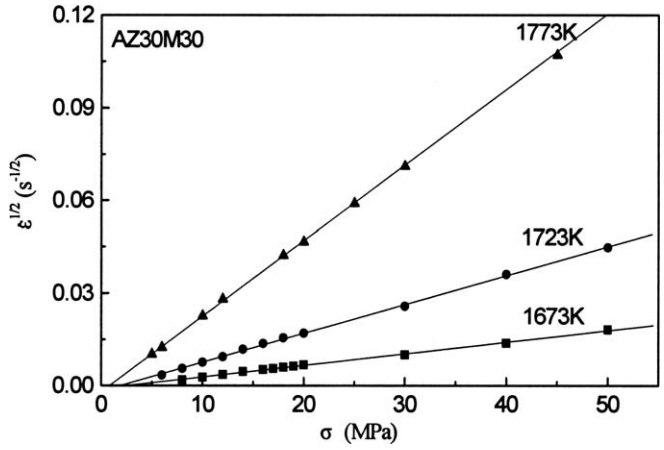

Fig. 6. Compensated strain rate $\dot{\varepsilon}^{-1/2}$ (where $n = 2.0$) plotted as a function of applied stress (σ).

It has been suggested that for metallic superplastic alloys, the origin of threshold stress is related to the segregation of impurity atoms at grain boundaries and their interaction with grain boundary dislocation motion [27]. Impurity segregation at boundaries is a well-documented phenomenon in ceramics, for instance, segregation of Zr [36], Y^{3+}, and La^{3+} [42] along Al_2O_3 boundaries, and Si [43], Y^{3+}, and Al^{3+} [44] along 3Y-TZP boundaries. The grain boundary width of impurity segregation was estimated to be up to several nanometers for silica doped 8Y-CSZ by Martin and Mecartney [45]. Although all starting materials are high purity, segregation of impurities along boundaries is inevitable due to the nature of multiphase ceramic composites. The segregation of impurities along boundaries will change the flow stress and the strain rate and it is well known that the impurity segregation can dramatically change the strain rate of pure alumina. For example, the strain rate of 1000 ppm zirconium-doped alumina is one order of magnitude lower than that of pure alumina [36]. Segregation also affects the strain rate in 3Y-TZP, depending on the doped ions [44].

As documented elsewhere [46], the segregation of impurities can be described by the following equation:

$$C = C_0 \exp(E/RT) \tag{1a}$$

where C is the concentration of impurities ions in the boundary, C_0 is the average concentration of impurity, E is the binding energy between the impurity ions and boundary dislocations, and T is the absolute temperature. Consistent with Eq. (1a) is the finding that the threshold stress for superplastic flow in Zn–22% Al [28,47] obeys the following equation:

$$\sigma_0/G = B_0 \exp(Q_0/RT) \tag{1b}$$

where B_0 is a constant, and Q_0 is an energy term. According to Eqs. (1a) and (1b), an increase in temperature will reduce impurity concentration at boundaries, which in return results in a decrease of threshold stress. Chaudhury et al. [28,47] extensively studied the effect of impurities on superplastic flow in Zn–22% Al and reported a similar trend: a decrease in the value of the threshold stress with an increase in temperature. Dominguez-Rodriguez et al. [48] have correlated an increase in threshold stress in TZP with decreasing temperature and increasing grain size. Recently, Morita et al. [17,41] also reported the threshold stress in 3Y-TZP, but no information about the temperature dependence of threshold stress was available in their work. In order to examine whether the data on the threshold stress for deformation in AZ30M30 obey Eq. (1b), the shear modulus of the material needs to be estimated. Due to the absence of direct measurements on the shear modulus of AZ30M30, the modulus was calculated using the following approximate procedure. For zirconia (3Y-TZP), the temperature dependence of the shear modulus (in MPa) was determined as [49]

$$G = 84 \times 10^3 - 13.3T \quad (2)$$

Using Eq. (2) yields $G = 61.8$ GPa at 1673 K, 61.1 GPa at 1723 K, and 60.4 GPa at 1773 K. For alumina, the shear moduli at 1673 and 1773 K were reported to be 137 and 135 GPa, respectively [50]. The elastic moduli of mullite were approximated to be 120 GPa at 1673 K, 118 GPa at 1723 K, and 116 GPa at 1773 K, respectively [51]. Using the simple approximation that $G = E/2(1+v)$ and $v = 0.28$, the shear moduli of mullite were estimated to be 46.9 GPa at 1673 K, 46.1 GPa at 1723 K, and 45.3 MPa at 1773 K. By adopting the mixture rule, as a first approximation, the shear moduli for AZ30M30 are estimated to be 86.5 GPa at 1673 K, 85.7 GPa at 1723 K, and 84.8 GPa at 1773 K. In Fig. 7, the estimated values of (σ_0/G) are plotted as the logarithm of (σ_0/G) against $1/T$. As seen from the figure, the data for AZ30M30 fall very close to a straight line, in agreement with Eq. (1b). The value of Q_0 inferred from the slope of the plot in Fig. 7 is 170 kJ/mol. According to Eqs. (1a) and (1b), this value of Q_0 should represent the binding energy for an impurity ion at boundaries. However, no values for the binding energies between impurity ions and boundaries in ceramics are documented for the purpose of comparison. An apparent threshold stress has also been observed in magnesium aluminate spinel [52]. The nonlinear threshold stress was attributed to electrical double barrier layers present at interfaces in that non-stoichiometric ceramic, formed due to charge compensation [52]. This explanation would apply also to this complex AZ30M30 system, where the majority of interfaces are also non-stoichiometric grain boundaries.

Under the condition of the presence of a threshold stress, the creep behavior of AZ30M30 in region II ($n \approx 2$) and region I ($n > 2$) may be described by a rate equation of the following form (modified power law creep):

$$\dot{\varepsilon} = A((\sigma - \sigma_0)/G)^2 \exp(-Q_c/RT) \quad (3)$$

where A is a constant that depends on temperature and microstructure (e.g., grain size). Eqs. (1b) and (3) offer an explanation for two experimental trends: (a) the variation in the apparent activation energy, Q_a, with applied stress, and (b) the decrease in the apparent stress exponent for creep in the low stress region (region I) with increasing temperature.

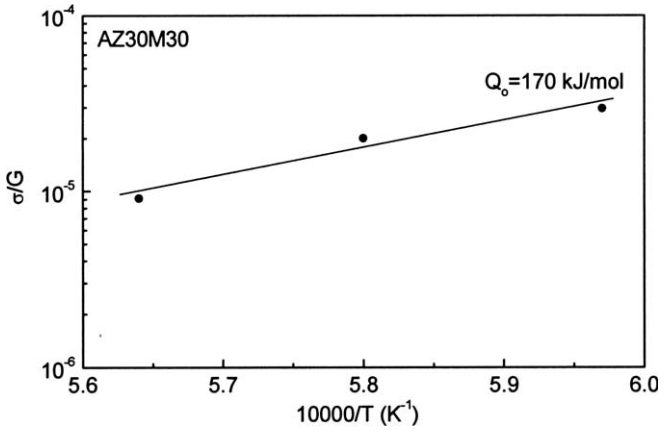

Fig. 7. Temperature dependence of the normalized threshold stress, σ/G, for AZ30M30.

Fig. 1(b) shows that apparent activation energy for creep increases with decreasing applied stress. Such a trend is in full agreement with that predicted by the following equation, which was developed [28] by combing Eqs. (1b) and (3) and the definition of the apparent activation energy

$$Q_c = Q_a - nQ_0/((\sigma/\sigma_0) - 1) \quad (4a)$$

It is possible to correct the apparent activation energy for the effect of the presence of a threshold stress using Eqs. (4). The results after correction as plotted in Fig. 1(b) indicate that the value of the true activation energy is essentially constant over the entire stress range (regions I and II) and is equal to about 870 kJ/mol. Based on extensive data available for superplasticity, this value of 870 kJ/mol should correspond to that for boundary diffusion in AZ30M30. However, no diffusion data are available for this complex material in order to verify this expectation. This material contains not only three types of grain boundaries between same phases but also three types of interface boundaries between different phases.

It was mentioned that the value of the apparent stress exponent for creep in the low-stress region (when the data are fitted by straight lines) decreases from 3.1 to 2.5 with increasing temperature from 1673 to 1773 K. This trend is predicted from the following equation [28] that was based on applying the definition of the apparent stress exponent to Eq. (4b) and using Eq. (1b)

$$n_a = n/(1 - \sigma_0/\sigma) \quad (4b)$$

With an increase in temperature, σ_0 decreases (Eq. (1b)), leading to a decrease in the apparent stress exponent for creep in the low stress region (region I) with increasing temperature.

The creep data obtained for AZ30M30 at various temperatures are logarithmically plotted as temperature compensated creep rate, $(\dot{\varepsilon}kT)/(Gb\exp-(Q/RT))$, versus normalized effective stress, $(\sigma - \sigma_0)/G$ in Fig. 8. As seen in this figure, the data cluster about a straight line whose equation describes the creep behavior of the alloy and whose slope is 2.

The threshold stress approach adopted in explaining deformation flow in ceramics was questioned and ruled out [32,33] for two reasons: (a) calculations yielded a negative threshold stress, and (b) a lower stress exponent was measured in the low-stress region. When the applied stress is low and close to the threshold stress, the strain rate is very sensitive with the change of load. It is not easy to collect the precise strain rate under this situation. However, the constant stress compressive test employed in the present study has the advantage of collecting the strain rate under controlled stress. Using the widely reported stress exponent of 2 that also characterizes the creep behavior of AZ30M30 in region II, the plotted strain rate raised to

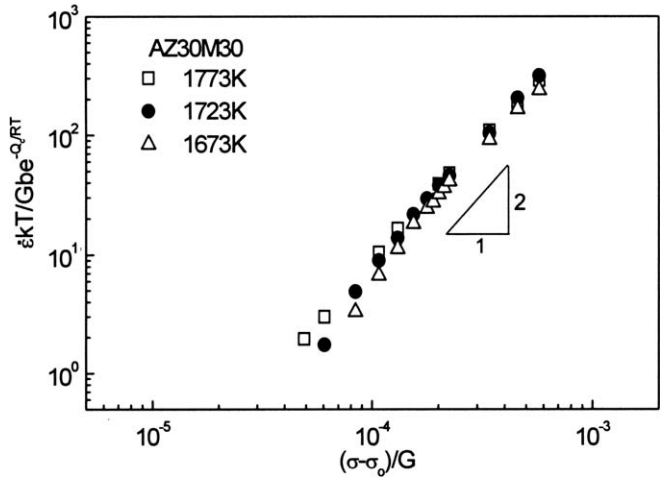

Fig. 8. Plot of normalized strain rate as a function of normalized effective stress on a double logarithmic scale.

a power of (1/2) versus applied stress on a linear scale yielded a positive threshold stress, which decreases with increasing temperature according to Eq. (1b). Such a trend is similar to those reported for superplastic metals such as Zn–22% Al [28,46]. The study of 3Y-TZP and 8Y-CSZ reported a decrease of stress exponent in the low-stress region, unlike the increase of stress exponent in the low-stress region in metals. Morita et al. [41] showed that the corrected strain rate due to grain boundary sliding resulted in the increase of stress exponent in the low-stress region for TZP. So the plot of strain rate without correction versus stress shows a similar trend to that in metals.

In summary, the increase in both the stress exponent and the apparent activation energy with decreasing applied stress (Fig. 1), the measurement of positive threshold stress values (Fig. 6), the temperature dependence of threshold stresses on temperature (Fig. 7), and the coalescence of the creep rates at various temperatures into a single line with slope of about 2 when plotted logarithmically against $(\sigma - \sigma_0)/G$ (a normalized effective stress) (Fig. 8) suggest a threshold stress approach is applicable to the description of the creep behavior of AZ30M30.

4.2. Deformation mechanism

It is well documented that grain boundary sliding is responsible for producing the strain during superplastic deformation in metallic systems. Recently, studies [53–56] were performed to assess the contribution of boundary sliding to deformation in submicrometer-size ceramics. The results of investigations on fine-grained alumina–zirconia ceramic composites [53] and polycrystalline alumina [54] have shown that the contribution of grain boundary sliding to the total strain is up to 80%. Also, direct evidence for grain boundary sliding has also been reported using SEM [55,56]. Although no attempt was made in the present study to measure boundary sliding in AZ30M30, the finding that grains remained essentially equiaxed even after large deformation and that dislocation activity is confined to some grains leads to the following deduction: boundary sliding plays the key role in the deformation process controlling the creep behavior of the material.

The occurrence of grain boundary sliding requires an accommodation process at grain boundary triple points or ledges. In general, there are several possible accommodation processes including boundary migration, dislocation motions, diffusion-related flow, or cavitation. In the present study, even after 100% deformation, there is no evidence of cavitation. Although conducting experiments under the condition of compression do not favor cavity formation, some cavities would have been observed if cavitation had served as a major accommodation process for boundary sliding. In addition, the maintenance of the equiaxed grain shape, the occurrence of limited grain growth, and the observation of dislocation activity in some grains in the deformed materials suggest that neither diffusional flow nor grain boundary migration significantly contributes as an accommodation process for boundary sliding during the superplastic deformation of AZ30M30. In addition, the contribution to the total strain from diffusion will be limited due to the nature of the multiphase ceramic composite and the lack of boundaries between similar phases. This inference is consistent with that related to the superplastic deformation of metallic systems. For example, the results of experiments on micrograin superplasticity in a Cu alloy [57] and Pb–62% Sn [58] have indicated that the contribution of diffusional flow to deformation in region II ($n \approx 2$) is not significant. Furthermore, it has been reported that cavitation is not present in high-purity Zn–22% Al when tested in tension [59].

The preceding discussion leads to the conclusion that dislocation motion plays the key role in accommodating grain boundary sliding AZ30M30. Several models [7–9] that are based on the concept of dislocation-accommodated boundary sliding have been developed. Of these models, the model by Ball and Hutchison [7] appears to be consistent with very recent substructural evidence reported for the superplastic Zn–22% Al alloy [15,60]. This model is based on the concept that although during high-temperature deformation grains can slide, rotate, or rearrange their position to enable deformation, not every grain can participate in grain boundary sliding. Rather, other grains that are unfavorably oriented or with irregular grain shapes could obstruct the easy relative motion of groups of grains that are sliding under applied stress. Thus, the shear stress becomes concentrated at any grain, triple point, or protrusion that obstructs motion of group. This local high stress can then generate dislocations in the blocking grain. The generated lattice dislocations traverse the blocking grain and pile-up against the opposite grain boundary. Then, dislocations climb into or along boundaries [61]. In the model, it was assumed that the average stress concentrated over the blocking grain, σ_c, to a first approximation, was related to applied stress, σ_a, by the following expression:

$$\sigma_c = R\sigma_a \quad (5)$$

where R is the ratio between the numbers of easy-sliding grain to blocking grains. By comparing the experimental data for Zn–22% Al that were obtained using an Instron tensile machine operated at constant crosshead speed with the final expression of the model, Ball and Hutchison [7] inferred that the value of $R = 4$. However, a comparison between the steady-state creep rates measured in creep experiments on Zn–22% Al [28,46] and those predicted from the model [7] shows that the former rates are faster than the later rates by at least one order of magnitude. This finding suggests that R may be larger than 4.

There are several features that are noted in the present study and that are relevant to dislocation-accommodated sliding by groups of grains. First, the highest density of dislocation found in mullite grains is probably not only because it is the softer phase with a much lower elastic modulus than that of alumina but also because it has complicated grain shape compared to zirconia and alumina grains. The non-uniform grain shape results from the processing on the original materials when mullite is formed by the reaction of amorphous SiO_2 and nanocrystalline Al_2O_3. The irregular mullite grain shape is more difficult to accommodate during grain boundary sliding. At irregular junctions high-stress concentrations develop. Second, dislocations are found in some grains, but not in every grain even when specimens were extensively tilted to a variety of $g \cdot b$ conditions during TEM operation. Dislocations, more often than not, are associated with grain junctions and grain boundaries, where high-stress concentrations are exerted from the preexisting grain boundary sliding. In addition, most dislocations were found to exist within the grains. Dislocations at the grain mantle region, as proposed by Gifkins [9] were observed, but this is not the most frequent dislocations feature in the current material. Most of the revealed dislocations at the boundary or mantle region were associated with zirconia grains. Third, the lack of tangles of dislocations, which is similar in trend to that observed in Zn–22% Al [15,60], suggests the occurrence of single slip in the grain. This finding is consistent with the creep behavior of the material. If the dislocations were tangled and pinned, it would cause strain hardening and an increase in the flow stress, a trend that is not observed. On the other hand, this also indicates dislocations are moving during deformation and acting as the accommodation process to grain boundary sliding.

The present study provides evidence for dislocation activities in some of the grains, especially those of mullite after deformation. Such evidence implies that dislocations are generated in these grains and then move to boundaries where they climb. It is appropriate to examine the generation of these lattice dislocations in the light of knowledge on dislocation theory.

The shear stress necessary to generate dislocations may be give by the following equation [62]:

$$\tau = \frac{Gb\{(1 - 3\nu/2)\ln(L/b) - 1 + \nu/2\}}{2\pi L(1 - \nu)} \quad (6)$$

where L is the distance between pinning points, ν is Poisson's ratio (=1/3), and b is the Burgers vector. The above equation is applied to mullite since there is clear evidence regarding dislocation activity in some of its grains. For this material, the Burgers vector, b, is not known, but on the basis of consideration of data available on ceramics, b can be assumed to be 0.4 nm. By substituting $L = d/3$, $d = 0.4$ mm, $b = 0.4$ nm, $\nu = 1/3$, and $G = 45$ MPa in Eq. (6), it is predicted that a normal stress, $\sigma(\sigma - 2\tau)$ of about 132 MPa is needed to generate lattice dislocations in mullite. Similar calculations can be performed for zirconia, in which dislocations were also found. In this case, using $b = 0.36$ nm and $G = 62$ MPa along with the other values used for mullite leads to $\sigma = 184$ MPa. The value of 184 MPa is close to 135 MPa reported by Balasubramanian and Langdon [10], who estimated the stress required to generate dislocation in zirconia using a slightly different equation.

The present calculations along with those of Balasubramanian and Langdon [10] show the presence of very large discrepancies in value between the stresses required to generate dislocation (Eq. (6)) and those actually applied. For example, the stress required to generate dislocations in mullite is 4 times higher than the applied stress of 30 MPa, which was used to test samples for substructural examination, and is 22 times higher than the lowest stress used in the investigation (6 MPa). Taking $b = 0.3$ or 0.5 nm does not significantly affect this finding. For $b = 0.3$ or 0.5 nm, the estimated stresses are 18 or 26 times, respectively, higher than the lowest stress used.

However, despite the above apparent discrepancy, a conclusion can be convincingly made that dislocation motion plays a role in accommodating grain boundary sliding in AZ30M30 for the following reasons. First, the stress in Eq. (6) does not necessarily represent applied stress as defects along boundaries or within the grains can act as stress concentrations. For example, as mentioned above, in the model of Ball and Hutchison [7], the sliding of a group of grains as a unit is blocked by an obstructing grain. This process leads to the generation of a high-stress concentration in the blocking grain, which was reflected in the incorporation of a stress "raiser", R, in the analysis of the model. It is difficult to estimate the exact level of such a high-stress concentration but it appears on the basis of present experimental evidence that it is high enough to generate dislocations. Such evidence, which is in full agreement with that most recently reported for the superplastic Zn–22% Al containing dispersion particles [15,60], is manifested by the presence of dislocations in some grains after creep deformation and the absence of dislocations the as-sintered materials. Second, even in metallic systems for which experimental evidence [15,57,58,60] has persuasively implied that dislocation activity is primarily responsible for providing the accommodation process for sliding, present calculations

reveal a discrepancy between applied stress and the stress required to generate dislocations. For example, when Eq. (6) is applied to Zn–22% Al using: $d = 2.5$ μm, $L = d/3$, $b = 0.27$ nm, $G = 35$ MPa [63], the shear stress required to generate dislocations is about 8.5 MPa. This value is much higher than the lowest shear stress (0.4 MPa) used in testing high-purity Zn–22% Al [28], in which region II (the superplastic region: $n \approx 2$) extends to the lowest strain rate without evidence for the presence of region I (low-stress region); the calculated stress is a factor of about 20 higher than the lowest applied. Thus a stress concentration of the order of 20 is reasonable to expect.

The results of this paper offer clear experimental evidence that superplastic deformation in this ceramic system, similar to metallic systems, involves dislocation-accommodated grain boundary sliding. Such evidence is manifested in the following findings: (a) TEM observations of dislocations that were generated during deformation; (b) the observation of parallel dislocations emanating from multiple grain junctions and traversing the grain boundary without forming dislocation tangles, indicating single slip; (c) the similarity of such dislocations in terms of configuration and arrangement to those observed in metallic superplastic system such as Zn–22% Al, for which dislocation assisted grain boundary sliding is an accepted mechanism [15,60]; and (d) calculations indicating that the stress concentrations at the irregularly shaped grain boundaries can magnify the applied stress high enough to cause slip in these ceramic materials. The aforementioned findings clearly refute earlier statements that dislocation activity should be disregarded as playing a critical role in accommodating grain boundary sliding in ceramics because no evidence of such dislocation activity has been documented [30].

5. Conclusions

(1) For AZ30M30, the plot of creep rate against applied stress on a logarithmic scale reveals the presence of two region of creep behavior, depending on the value of applied stress: regions II and I. In region II (high stresses), the stress exponent, n, is about 2 and the activation energy approaches a value of 870 kJ/mol. In region I (low stresses), $n > 2$ and the apparent activation energy is not only higher than 870 kJ/mol but also increases with decreasing stress. Regions II and I are similar, in terms of the variation in both the stress exponent and the apparent activation energy with applied stress, to the intermediate-stress region and the low-stress region, respectively, that characterize the sigmoidal relation between stress and strain rate in superplastic metallic alloys.

(2) An analysis of the creep data yielded a positive threshold stress, which decreases with increasing temperature.

(3) When the creep rates of AZ30M30 obtained at various temperatures are plotted against $(\sigma - \sigma_0)/G$ (a normalized effective stress) on a logarithmic scale, the data coalesce into a single straight line with slope of about 2, suggesting that a threshold stress approach is applicable to the description of the creep behavior of the material and that regions II and I arises from the same deformation mechanism.

(4) Evidence for dislocation activity was found in deformed specimens. The dislocation density is highest in mullite and lowest in alumina. There were only a few isolated dislocations in the as-sintered state, so the dislocations must have been generated during high-temperature deformation.

(5) Dislocations are often found within the grains, but not as frequently at the mantle regions. In addition, dislocations were not present in every grain. This observation is consistent with the concept that a group of grains slide as a unit until blocked by an unfavorably oriented grain.

(6) The occurrence of boundaries sliding during superplastic flow is primarily accommodated by lattice dislocation motion. These lattice dislocations appear to be generated not by applied stresses but rather by local stresses, which are much higher than the former stresses as a result of the presence of stress concentrations.

Acknowledgements

This work was supported by the Division of Materials Research of the National Science Foundation under Grant No. 0207197. Also, one of us (F.A.M.) would like to acknowledge the support of the National Science Foundation under Grant No. 0304629.

References

[1] Wakai F, Sagaguchi S, Matsuno Y. Adv Ceram Mater 1986;1:259.
[2] Wakai F, Kato H. Adv Ceram Mater 1988;3:71.
[3] Kajihara K, Yoshizawa Y, Sakuma T. Acta Mater 1995;43:1235.
[4] Dillon RP, Sosa SS, Mecartney ML. Scr Mater 2004;50:1441.
[5] Kim BN, Hiraga K, Morita K, Sakka Y. Nature 2001;413:288.
[6] Bengough GD. JIM 1912;7:123.
[7] Ball H, Hutchinson MM. Mater Sci 1969;3:1.
[8] Mukherjee AK. Mater Sci Eng 1971;8:83.
[9] Gifkins RC. Metall Trans A 1976;7:1225.
[10] Balasubramanian N, Langdon TG. Scr Mater 2003;48:599.
[11] Muñoz A, Wakai F, Rodríguez AD. Scr Mater 2001;44:2551.
[12] Lorenzo-Martín C, Gómez-García D, Gallardo-López A, Domínguez-Rodríguez A, Chaim R. Scr Mater 2004;50:1151.
[13] Tekeli S, Davies TJ. J Mater Sci 1998;33:3267.
[14] Bataille A, Crampon J, Duclos R. Ceram Int 1999;25:215.
[15] Xun Y, Mohamed FA. Acta Mater 2004;52:4401.
[16] Morita K, Hiraga K. Philos Mag Lett 2001;81:311.
[17] Morita K, Hiraga K. Acta Mater 2002;50:1075.
[18] Duclos R, Crampon J. Philos Mag Lett 2002;82:529.
[19] Morita K, Hiraga K, Kim BN, Suzuki TS, Sakka Y. J Am Ceram Soc 2004;87:1102.
[20] Morita K, Kim B-N, Hiraga K, Sakka Y. Philos Mag Lett 2003;83:533.
[21] Moon WJ, Ito T, Uchimura S, Saka H. Mater Sci Eng A 2004;387:837.

[22] Mohamed FA, Langdon TG. Acta Metall 1975;23:117.
[23] Johnson HR. Metals Rev 1970;15:115.
[24] Burton B. Scripta Metall 1971;5:669.
[25] Ashby MF, Verrall RA. Acta Metall 1973;21:149.
[26] Gittus JH. J Eng Mater Technol 1977;99:244.
[27] Mohamed FA. J Mater Sci 1983;18:582.
[28] Chaudhury PK, Mohamed FA. Acta Metall Mater 1988;36:1099.
[29] Bravo-Leon A, Jimenez-Melendo M, Dominguez-Rodriguez A, Chokshi AH. Scripta Metall 1996;34:1155.
[30] Gomez-Garcia D, Lorenzo-Martin C, Munoz-Bernabe A, Dominguez-Rodriguez A. Philos Mag 2003;83:93.
[31] Gomez-Garcia D, Lorenzo-Martin C, Munoz-Bernabe Z, Dominguez-Rodriguez A. Phys Rev B 2003;67:144101.
[32] Owen DM, Chokshi AH. Acta Mater 1998;46:667.
[33] Berbon MZ, Landon TG. Acta Mater 1999;47:2485.
[34] Chen T, Mecartney ML. J Mater Res 2005;20:13.
[35] Chen T, Mecartney ML. J Am Ceram Soc 2005;88:1004.
[36] Wakai F, Takayuki N, Takeo I. J Am Ceram Soc 1997;80:2361.
[37] Wang ZC, Davis TJ, Ridley N. Scr Metall Mater 1993;28:301.
[38] Morita K, Hiraga K. Scr Mater 2003;48:1403.
[39] Yan S, Earthman JC, Mohamed FA. Philos Mag 1994;69:1017.
[40] Jimenez-Melendo M, Dominguez-Rodriguez A, Holgado-Slado M. Int J Plasticity 2001;17:341.
[41] Morita K, Kim BN, Hirage K, Sakka Y. Mater Sci Eng A 2004;387–389:655.
[42] Li YZ, Wang CM, Chan HM, Rickman JM, Harmer MP, Chabala JM, Gavrilov KL, Levi-Setti R. J Am Ceram Soc 1999;82:497.
[43] Nakatani K, Nagayama H, Yoshida H, Yamamoto T, Sakuma T. Scr Mater 2003;49:791.
[44] Ross IM, Rainforth WM, McComb DW, Scott AJ, Brydson R. Scr Mater 2001;45:653.
[45] Martin MC, Mecartney ML. Solid State Ionics 2003;161:67.
[46] Gleiter H, Chalmers B. Prog Mater Sci 1972;16:134.
[47] Chaudhury PK, Park KT, Mohamed FA. Metall Trans A 1994;25:2391.
[48] Dominguez-Rodriguez A, Bravo-Leon A, Ye JD, Jimenez-Melendo M. Mater Sci Eng A 1998;247:97.
[49] Hayakawa M, Miyauchi H, Ikegami A, Nishida M. Mater Trans JIM 1998;39:268.
[50] Munro RG. J Am Ceram Soc 1997;80:1919.
[51] Osendi MI, Baudín CJ. Eur Ceram Soc 1996;16:217.
[52] Lappalainen R, Pannikkat A, Raj R. Acta Metall 1993;41:1229.
[53] Clarisse L, Petit F, Crampon J, Duclos R. Ceram Int 1995;26:295.
[54] Chokshi AH. J Mater Sci 1990;25:3221.
[55] Duclos R. J Eur Ceram Soc 2004;24:3103.
[56] Sudhir B, Chokshi AH. J Am Ceram Soc 2001;84:2625.
[57] Falk LKL, Howell PR, Dunlop GL, Langdon TG. Acta Metall 1986;34:1203.
[58] Valiev RZ, Langdon TG. Acta Metall 1993;3:949.
[59] Park KT, Mohamed FA. Metall Trans 1990;21A:2605.
[60] Xun Y, Mohamed FA. Philos Mag 2003;83:2247.
[61] Friedel J. Dislocations. Pergamon Press; 1964. p. 315.
[62] Hirth JP, Lothe J. Theory of dislocations. New York (NY): McGraw-Hill; 1968.
[63] Mohamed FA, Shei SA, Langdon TG. Acta Metall 1975;23:679.